MEASUREMENT OF UNSTEADY AERODYNAMIC FORCES OF 3D FLAPPING WING IN HOVERING TO FORWARD FLIGHT

Hiroto Nagai*, Koji Isogai , Toshiyuki Hayase§**
***Kyushu Institute of Technology, **Nippon Bunri University, §Tohoku University**

Keywords: *Insect, Flapping Wing, Hovering, Forward Flight, Unsteady Aerodynamic Forces*

Abstract

We measured unsteady aerodynamic forces of a 3D flapping wing in hovering and forward flight using a dynamically scaled mechanical model in a water tunnel, and investigated effects of motion kinematics of a flapping wing on the aerodynamic characteristics. Two simple motion types were used for comparison; trapezoidal and sinusoidal types, whose time histories of angular velocities are represented as trapezoidal and sinusoidal functions, respectively. The results show that the trapezoidal type of flapping motion and the trapezoidal type of feathering motion with the shorter rotational time should be selected in order to obtain higher efficiency in both hovering and forward flight. In order to obtain larger lift, the sinusoidal type of flapping motion and the trapezoidal type of feathering motion should be selected in hovering and slower forward flight; and the sinusoidal type of flapping motion and the sinusoidal type of feathering motion should be selected in faster forward flight.

Nomenclature

b	semi-chord length at 2/3 semi-span
C_F	normal force coefficient
C_L, C_T	lift and thrust coefficients
C_P	power coefficient
f	flapping frequency
F_n	normal force to wing surface
J	advance ratio
k	reduced frequency
L, T	lift and thrust
l_r	reference semi-span length
M_t	torque around flapping axis
P	needed power for flapping motion
Re	Reynolds number
t^*	non-dimensional time ($= f \cdot t$)
U_0	forward velocity
V_0	reference velocity
η	propulsive efficiency
θ, θ_0	feathering angle and the amplitude
τ_r	non-dimensional rotational time
τ_t	non-dimensional reversal time
ϕ, ϕ_0	flapping angle and the amplitude
ψ	stroke plane angle

superscripts

$-$	time-averaged value
$*$	non-dimensional

1 Introduction

Many experimental and numerical researches have been conducted and clarified some of the unsteady aerodynamic phenomena in insect flights. In particular, measurements with a dynamically scaled mechanical model have presented reliable data and explained many phenomena, such as delayed stall, rotational effect, and wake capture [1, 2, 4]. Previous works of measurements of unsteady aerodynamic forces with a scaled model have been conducted in still water, which simulate hovering flight. Recently, Dickson and Dickinson [2] have conducted measurements of aerodynamic forces using a mechanical model translated horizontally in mineral oil, and

investigated the influence of advance ratio on the delayed stall. However, experiments which simulate forward flapping flights have not been conducted yet, although many numerical simulations have been made for forward flapping flight [5]. In addition, the effects of parameters which govern the aerodynamic characteristics of a flapping wing have not been investigated enough.

In this paper, measurements of unsteady aerodynamic forces of a 3D flapping wing are conducted with a scaled mechanical model in a water tunnel, which can simulate hovering and forward flight; in addition, we investigate the effects on aerodynamic characteristics between two simple motion types of flapping kinematics: trapezoidal and sinusoidal types.

2 Experimental Methods

2.1 Motion kinematics of a flapping wing

The three-dimensional orthogonal coordinate systems of a flapping wing are presented in Fig.1. The origin O is at the base of the right wing; Z is in the vertically downward direction; and X is in the direction of the forward flight. The z-axis is a flapping axis; and the x-y plane is a stroke plane. While the stroke plane is horizontal in hovering, it is tilted at an angle ψ around the Y-axis in forward flight. The y_w-axis is a span axis of wing and the z_w-axis is parallel to the wing chord direction, which are fixed with the wing. A flapping angle ϕ is defined as the angle between the y_w-axis and the y-axis; and a feathering angle θ is defined as the angle between the z_w-axis and z-axis.

The aerodynamic force normal to the wing F_n is divided into a vertical component, lift L, and a horizontal component, thrust T. Thus, the lift and thrust are related with F_n as follows:

$$L = F_n(\cos\psi\sin\theta - \sin\psi\cos\phi\cos\theta)\ , \quad (1)$$

$$T = F_n(\cos\psi\cos\phi\cos\theta + \sin\psi\sin\theta)\ . \quad (2)$$

In this study, we employed two simple types of flapping kinematics: a trapezoidal type and a sinusoidal type.

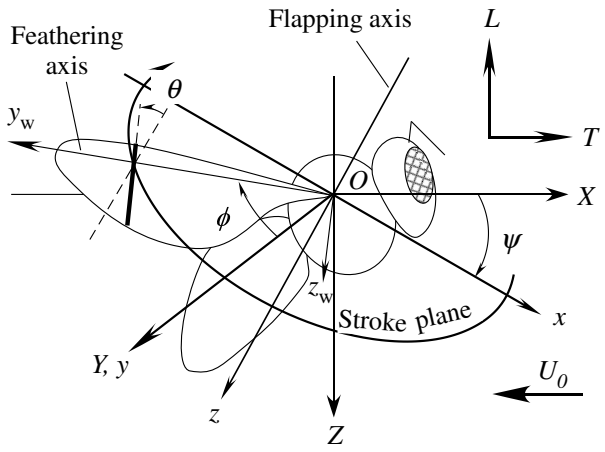

Fig. 1 3D-coordinate system of flapping wing.

In the trapezoidal type of motion kinematics, the time histories of angular velocity are represented as a trapezoidal function, as shown in Fig.2. The flapping motion of trapezoidal type can be divided into two phases: a flapping translational phase and a reversal phase. In the flapping translational phase, the wing moves at a constant flapping velocity. In the reversal phase, the wing decelerates and accelerates at a constant acceleration. The duration of the reversal phase is denoted by a reversal time τ_t. The feathering motion of trapezoidal type can be also divided into two phases: a feathering translational phase and a rotational phase. The wing moves at a constant angle of attack in the feathering translational phase; then, the wing rotates around the feathering axis in the rotational phase. The duration time of the rotational phase is represented by τ_r; and, the rotational acceleration time of the feathering motion is denoted by τ_a. In our experiments, τ_t was a constant of 0.2; τ_r was three kinds of 0.2, 0.3, and 0.4; and, $\tau_a = \tau_r/4$.

On the other hand, in the sinusoidal type of motion kinematics, the time histories of both angle and angular velocity are represented as sinusoidal functions. However, we could not use the sinusoidal function for the time histories of angular velocity because of the limitation of our motors. Therefore, we employed a trapezoidal function as an approximate function instead of the sinusoidal function. In order to minimize the dis-

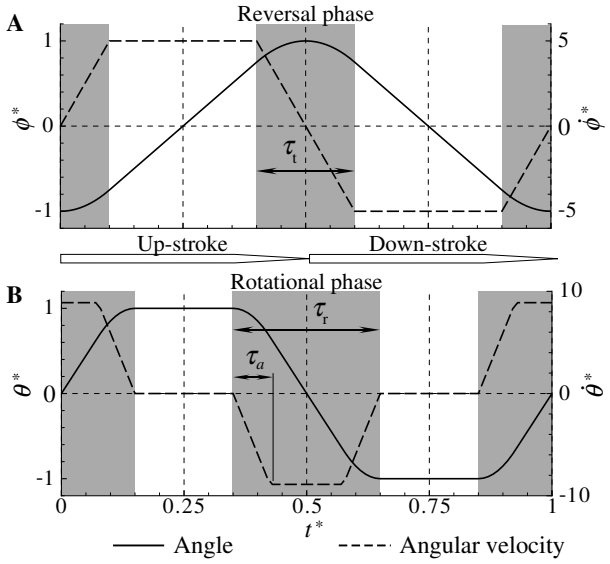

Fig. 2 Trapezoidal type of motion kinematics: (A) flapping motion and (B) feathering motion.

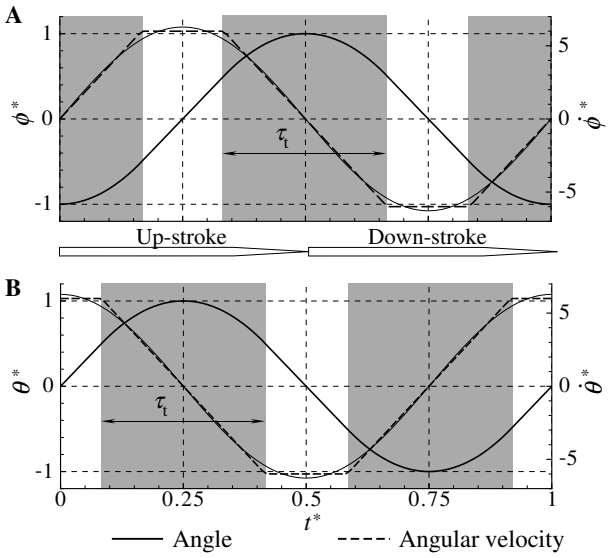

Fig. 3 Approximate sinusoidal type of motion kinematics: (A) flapping motion and (B) feathering motion.

crepancy of the time histories of angle between the approximate and real sinusoidal functions, we calculated the optimal acceleration time, which means τ_t in the trapezoidal type. As a result, if $\tau_t = 0.33$, then the time histories of angle of approximate sinusoidal function closely agrees with that of real sinusoidal function as shown in Fig.3.

All motions are the so-called *symmetrical motion* [1], in which the waveform of feathering motion is symmetrical at the reversals ($t^* = 0$ and 0.5), except for Fig. 9.

2.2 Experimental apparatus of scaled flapping model

We used a scaled mechanical model of flapping wing for measurements of unsteady aerodynamic forces. The scaled flapping apparatus is illustrated in Fig.4. The flapping and feathering motions were driven by two stepping motors, respectively. The two motions were controlled independently using a controller.

A rectangular beam, which was used as a force/torque transducer, connected the motor for feathering motion with the wing base. The rectangular beam mounted two sets of strain gages wired in two-active gage method, which were used for measuring bending moments at two locations. Although it is difficult to measure the distribution of fluid forces on the wing, we can calculate the total force acting on the wing by the gap of the bending moments at the two locations. We measured normal forces to the wing surface and torques around the flapping axis. It is well-known that the fluid force tangential to a thin flat flapping wing is very small compared with the normal fluid force [1]. In addition, the torque around the feathering axis is also very small compared with the torque around the flapping axis [3]. The torque around the flapping axis M_t were calculated by interpolation from the bending moments at the two locations. The aerodynamic power P needed for flapping motions are given by,

$$P = M_t \dot{\phi} \,. \tag{3}$$

Note that the measured forces and torques include the gravitational and inertial contributions in addition to the aerodynamic one. Therefore, we must subtract the gravitational and inertial forces and torques from the measured data. The gravitational contribution was measured in water at a very slow flapping frequency of 0.01 Hz; the

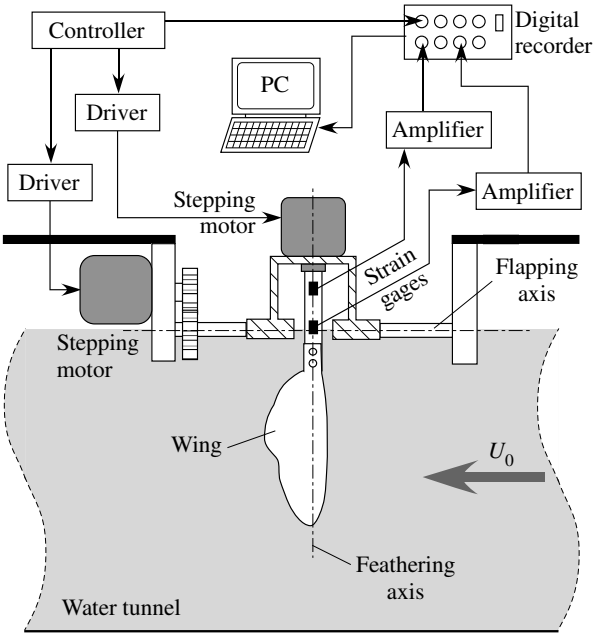

Fig. 4 Experimental apparatus of scaled flapping model.

inertial contribution was measured in air.

The flapping apparatus was placed over a water tunnel, and the water surface reached to the flapping axis. The water tunnel was 6 m long $\times$ 3 m wide in total size and had a test section with the size of 1.9 m long $\times$ 0.75 m wide $\times$ 0.38 m high.

The test wing had a span length l of 100 mm and was a thin flat plate with a thickness of 1 mm. In order to minimize the gravitational and inertial contributions, the test wing consisted of an acrylic plate embedded inside an aluminum frame. The planform of the test wing mimicked that of a bumblebee, *Bombus terrestris* (see Fig.5). The test wing was considered as a rigid wing because the deformation of the wing was very small.

Three non-dimensional parameters are required in order to achieve an accurate dynamic scaling of the forces obtained via the scaled model: the Reynolds number, reduced frequency, and advance ratio. A reference length b is defined as a semi-chord length at the 2/3 semi-span location. A reference velocity V_0 is defined based on

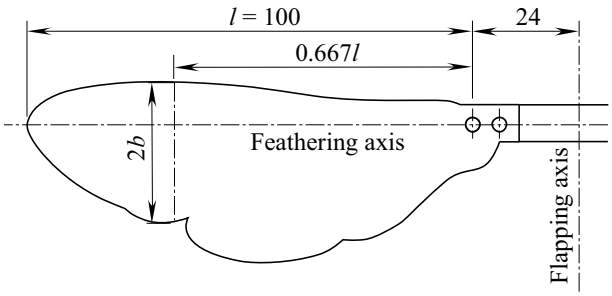

Fig. 5 Planform of test wing.

the flapping velocity, given by,

$$V_0 = 2\pi f \phi_0 l_r \ , \tag{4}$$

where the l_r is a reference semi-span length, f is a flapping frequency, and ϕ_0 is an amplitude of flapping motion. In our experiments, the wing base was placed at 24 mm apart from the flapping axis; therefore, $l_r = 2/3\ l + 24$ mm.

The Reynolds number, the reduced frequency, and the advance ratio are defined as follows, respectively:

$$Re = V_0 b/\nu \ , \tag{5}$$
$$k = 2\pi f b/V_0 \ , \tag{6}$$
$$J = U_0/V_0 \ , \tag{7}$$

where ν is a kinematic viscosity, and U_0 is a forward velocity. In our experiments, the amplitudes of flapping and feathering motions, ϕ_0 and θ_0, were fixed with 60° and 45°, respectively, based on the observation of the bumblebee [6]. The flapping frequency was in $0.2-0.5$ Hz; then, $Re = 1000-5000$ and $k = 0.166$.

The measured fluid forces and power are nondimensionalized as follows:

$$C_F = F_n/(0.5\rho V_0^2 S) \ , \tag{8}$$
$$C_L = L/(0.5\rho V_0^2 S) \ , \tag{9}$$
$$C_T = T/(0.5\rho V_0^2 S) \ , \tag{10}$$
$$C_P = P/(0.5\rho V_0^3 S) \ , \tag{11}$$

where S is a wing area, and ρ is a density of fluid. For flapping flight of insects, time-averaged forces through a cycle are important rather than

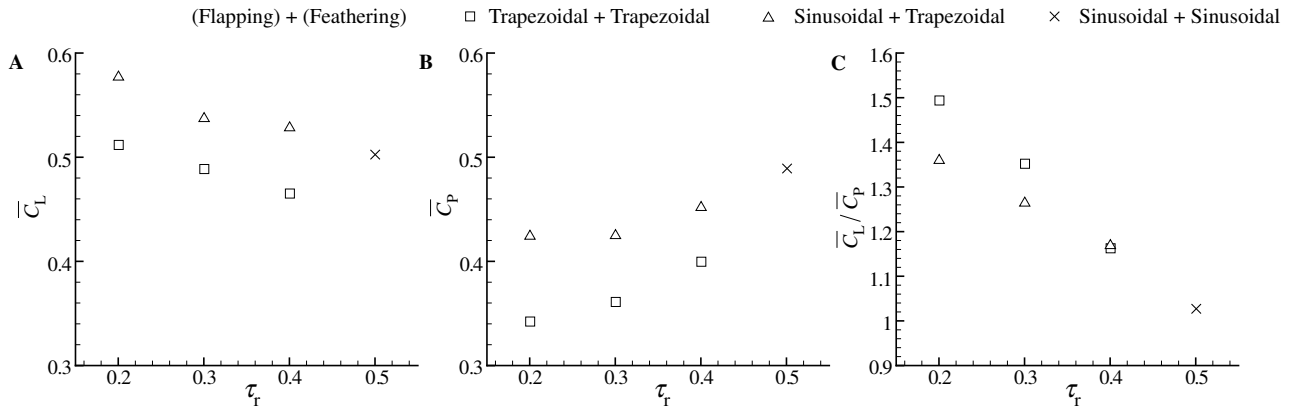

Fig. 6 Aerodynamic characteristics *vs* τ_r plotted by the motion types in hovering flight.

time-varying forces. The time-averaged coefficients are represented as $\bar{C_F}, \bar{C_L}, \bar{C_T}$, and $\bar{C_P}$. In order to compare the performance of flapping wing, we defined efficiency of a flapping wing. Propulsive efficiency is generally defined as,

$$\eta = \bar{T} U_0 / \bar{P} \,. \tag{12}$$

In hovering or horizontally forward flight, lift does not work against the body of insect because it does not move in the vertical direction. However, we consider the ratio of $\bar{C_L}/\bar{C_P}$ as the efficiency of lift in this study.

3 Aerodynamic characteristics in hovering flight

3.1 Comparison of motion types

In this section, the aerodynamic characteristics are compared between the motion types in hovering flight. We used three combinations of motion types; the first is the sinusoidal types in both flapping and feathering motions; the second is the sinusoidal type of flapping motion with the trapezoidal type of feathering motion; the third is the trapezoidal types of both flapping and feathering motions. Figure 6 shows the aerodynamic characteristics *versus* the rotational time plotted by each combination of motion type. It is considered that the sinusoidal type of feathering motion corresponds with $\tau_r = 0.5$ because it consists of only the rotational phases without any translational phase. In comparing between the two types of flapping motion, $\bar{C_L}$ and $\bar{C_P}$ in the sinusoidal type of flapping motion are larger than those in the trapezoidal type; however, $\bar{C_L}/\bar{C_P}$ in the sinusoidal type of flapping motion is smaller than that in the trapezoidal type. The result indicates that the sinusoidal type of flapping motion generates larger lift but needs much larger power, and, as a result, has the smaller efficiency than the trapezoidal type of flapping motion. In comparing between the two types of feathering motion, $\bar{C_L}$ increases; $\bar{C_P}$ decreases; and, as a result, $\bar{C_L}/\bar{C_P}$ increases with the shorter rotational time. The result indicates that the trapezoidal type of feathering motion with the shorter rotational time generates larger lift and needs smaller power, and, as a result, has the higher efficiency than the sinusoidal type of feathering motion.

3.2 Discussion of flapping motion type

The difference of aerodynamic characteristics between the two types of flapping motion can be explained as the difference of time histories of flapping velocity. Although the sinusoidal type moves the same displacement during a cycle as the trapezoidal type, it has the larger maximum velocity than the trapezoidal type instantaneously (see the dotted lines in Figs.2A and 3A). As a result, the sinusoidal type has a larger mean-squared velocity through a cycle, but has a much larger mean-cubed velocity than the trapezoidal type. It is clear that lift and power are pro-

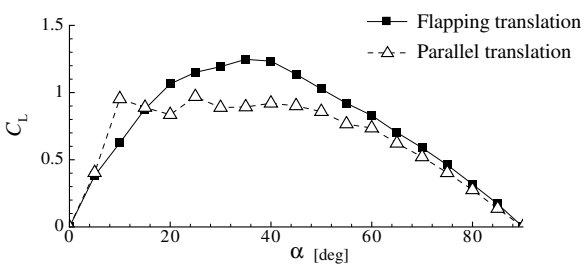

Fig. 7 Comparison of C_L *vs* α between parallel and flapping translation.

portional to the squared and cubed velocity, respectively, as shown in Eq.(11). Therefore, the sinusoidal type of flapping motion needs much more power though it generates more lift than the trapezoidal type.

This explanation agrees with the time-averaged results shown in Fig.6. For example, in comparing between the *sine-trapez* and *trapez-trapez* types with the same rotational time of 0.2 (i.e., with the same feathering motion), $\bar{C}_L$ and $\bar{C}_P$ in the *sine-trapez* type are 12% and 24% larger than those in the *trapez-trapez* type, respectively. On the other hand, the mean-squared and mean-cubed velocities in the sinusoidal type of flapping motion are 9% and 23% larger than those in the trapezoidal type of flapping motion. The increments of $\bar{C}_L$ and $\bar{C}_P$ agree well with those of the mean-squared and mean-cubed velocities.

In order to estimate the contribution of flapping velocity to lift, we measured the lift coefficient of the test wing against the angle of attack in flapping translation, in which the wing rotates around the flapping axis at a constant velocity and at a constant angle of attack. Figure 7 shows the relation of C_L with α, compared with that in the parallel translation. In the flapping translation, a leading-edge vortex is stably attached on the wing surface through the translation, called delayed stall [1]. Quasi-steady estimations of the contribution of flapping velocity to lift are calculated from the measured relation of C_L with α in the flapping translation, based on the instantaneous flapping velocity and angle of attack. Figure 8 show the time histories of C_L in the estima-

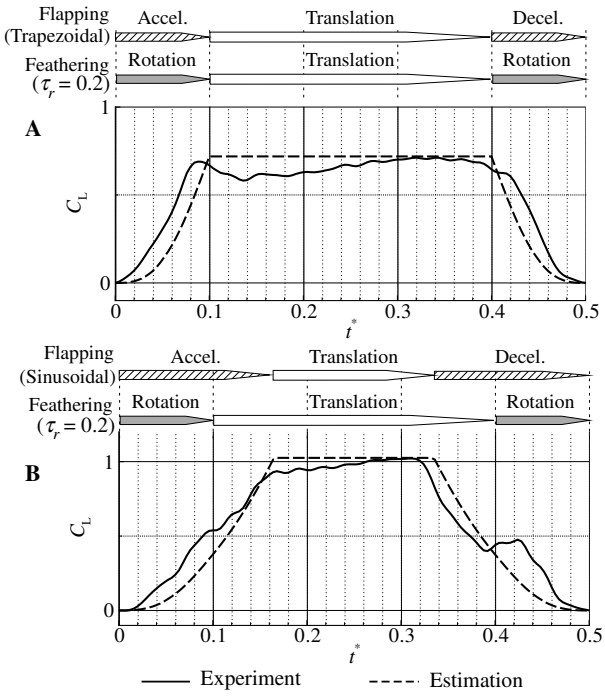

Fig. 8 Quasi-steady estimation of flapping translation: (A) *trapez-trapez* (B) *sine-trapez* type.

tions and experiments, with the same rotational time of $\tau_r = 0.2$ in the *trapez-trapez*type and *sine-trapez* type, respectively. The estimations agree well with the measured forces in both cases, in particular, through the translational phases. This result also indicates that the differences of aerodynamic characteristics are mainly attributed to the difference of flapping velocity between the two types of flapping motion. However, there are large discrepancies except for the translational phases. These discrepancies are due to the unsteady effects of the flapping and feathering motions, called the rotational effect and/or wake capture [1].

3.3 Discussion of feathering motion type

In order to investigate the rotational effect, an example is presented. Figure 9 shows the time histories of C_F in the up-stroke in the cases of *trapez-trapez* type in 10% advanced timing of rotation. The two cases have the same flapping motion and the different rotational time: $\tau_r = 0.2$ and 0.4. In $0.1 < t^* < 0.2$, the wing translates

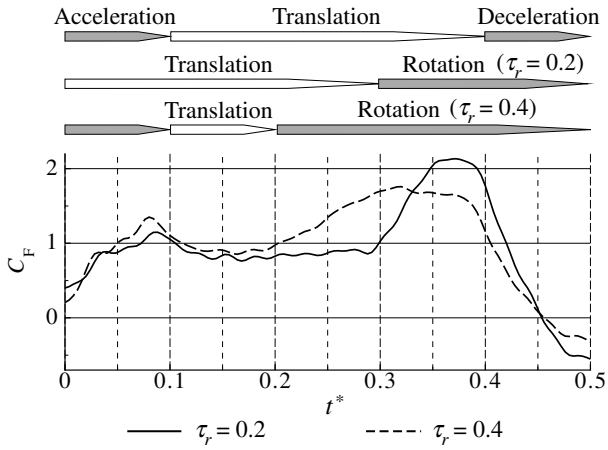

Fig. 9 Comparison of rotational effect between $\tau_r = 0.2$ and 0.4.

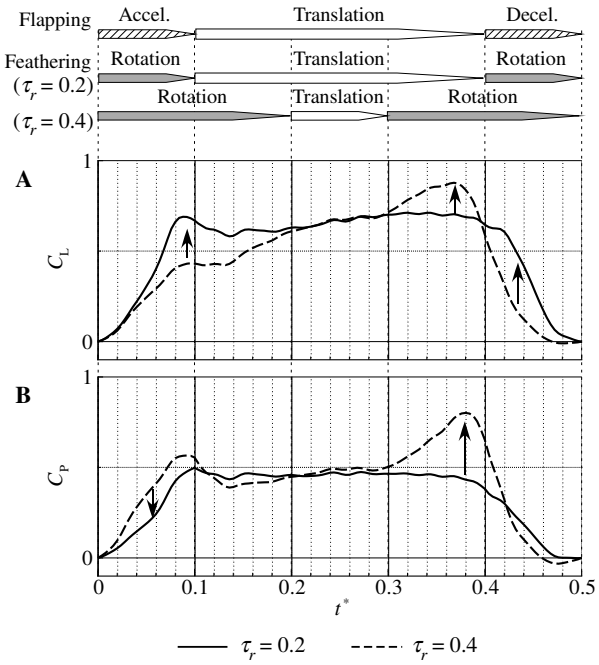

Fig. 10 Contribution of rotational effect to lift and thrust.

at the same velocity and the same angle of attack in both cases. In this range, C_F in both cases agree well, where the delayed stall effect plays a major roll. Once the rotational phase starts, C_F increases rapidly in both cases; then, once the deceleration starts, C_F decreases rapidly in both cases. Before the deceleration phase, C_F has a peak in each case. The maximum of C_F in $\tau_r = 0.2$ is 18% larger than that in $\tau_r = 0.4$. These results indicate that the normal force increases with the shorter rotational time, in other words, with the faster rotation.

The rotational effect does not always contribute to improve the performance of hovering flight. The timing of the rotational phase is important in order to obtain higher efficiency. Figure 10 shows the time histories of C_L and C_P in the up-stroke for the two cases: the *trapez-trapez* types in $\tau_r = 0.2$ and 0.4. The rotational phases in $\tau_r = 0.4$ overlap with the flapping translational phase in $0.1 < t^* < 0.2$ and $0.3 < t^* < 0.4$; on the other hand, those in $\tau_r = 0.2$ completely correspond with the flapping reversal phase.

First, let us discuss the combination of the rotational phase with the flapping translational phase, (i.e., $0.3 < t^* < 0.4$ and $0.1 < t^* < 0.2$ in the case of $\tau_r = 0.4$). As shown in $0.3 < t^* < 0.4$ in Fig.10, C_L and C_P of $\tau_r = 0.4$ rise rapidly and have peaks because of the enhanced normal force due to the rotational effect. However, the increment of C_P due to the rotational effect is larger than that of C_L; as a result, the efficiency decreases. This is because the enhanced normal force vector due to the rotational effect is directed to the stroke plane (horizontal in hovering) by the pitching-up of wing, which causes the increases of flapping torque and power. Similarly, the last quarter of the rotational phase of $\tau_r = 0.4$ ($0.1 < t^* < 0.2$), causes the decrease of C_L rather than that of C_P, which results in the decrease of efficiency.

Next, let us discuss the combination of the rotational phase with the flapping reversal phase, (i.e., $0.4 < t^* < 0.5$ and $0.0 < t^* < 0.1$). As shown in Fig.10, the increment of C_L in $\tau_r = 0.2$ is larger than that of C_P in $0.4 < t^* < 0.5$. C_L in $\tau_r = 0.2$ is larger than that in $\tau_r = 0.4$ although C_P in $\tau_r = 0.2$ is smaller than that in $\tau_r = 0.4$ in $0.0 < t^* < 0.1$. These results indicate that the rotational phase during the reversal phase contributes to the increase of lift rather than power, which results in the increase of efficiency.

In summary, the rotational phase during the flapping translational phase causes the decrease

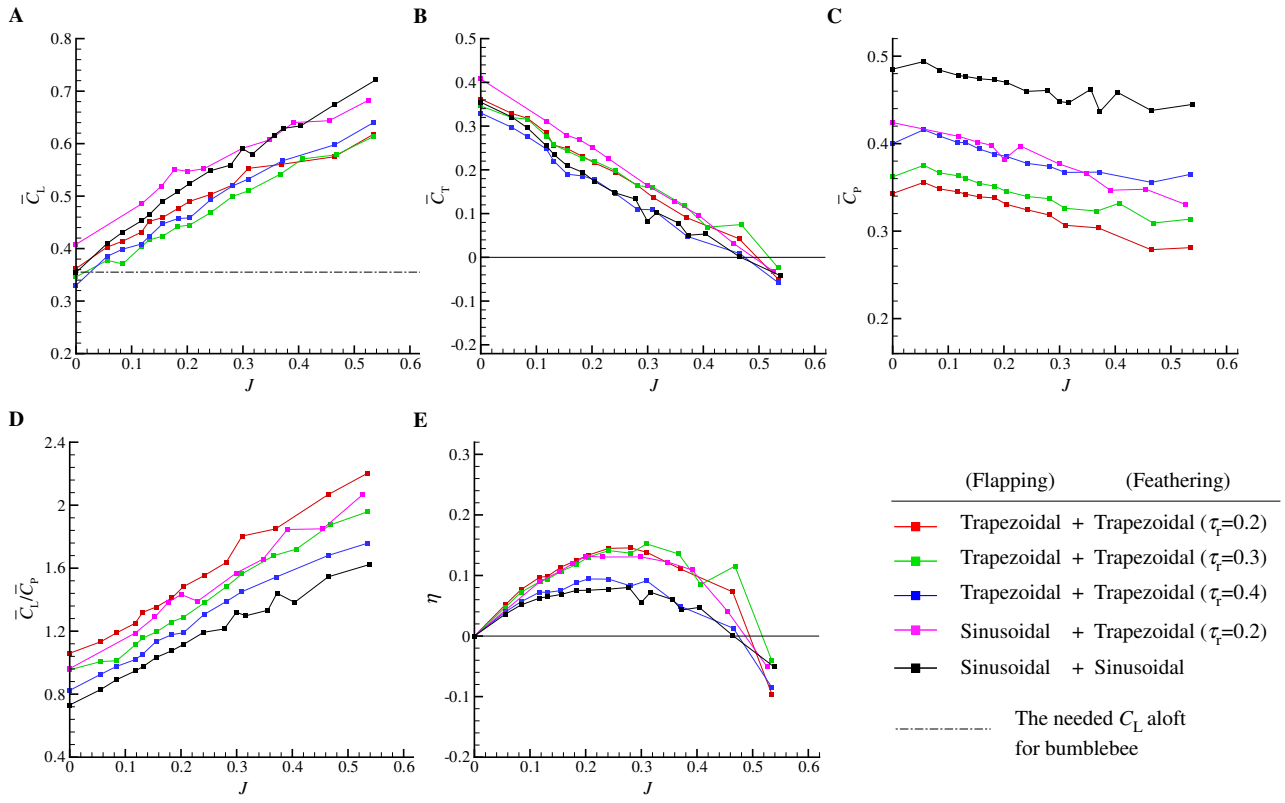

Fig. 11 Aerodynamic characteristics *vs* J at $\psi = 45^\circ$ plotted by the motion types.

of the efficiency; on the contrary, the rotational phase during the reversal phase contributes to the increase of the efficiency.

4 Aerodynamic characteristics in forward flight

4.1 Comparison of motion types

In this section, the aerodynamic characteristics are compared between the motion types in forward flight. Figure 11 shows the relations of the aerodynamic characteristics with the advance ratio plotted by each combination of motion types at the stroke plane angles of $\psi = 45^\circ$.

As shown in Fig.11A, $\bar{C_L}$ increases with the shorter rotational time in the *trapez-trapez* types at the low advance ratios, just like in hovering flight. However, there are different tendencies from in hovering flight at the high advance ratios; for example, $\bar{C_L}$ in $\tau_r = 0.4$ becomes larger than that in $\tau_r = 0.2$; $\bar{C_L}$ of the *sine-sine* type is larger than that of the *sine-trapez* type though it is smaller at the low advance ratios. These results indicate that the increasing rate of $\bar{C_L}$ with respect to the advance ratio is larger with the longer rotational time.

As shown in Fig.11B, the decreasing rate of $\bar{C_T}$ with respect to the advance ratio is larger with the shorter rotational time. For example, $\bar{C_T}$ in $\tau_r = 0.2$ is larger than that in $\tau_r = 0.3$ at the low advance ratios; however, it is smaller at the high advance ratios. All cases of motion types become negative thrust about $J > 0.5$. As shown in Fig.11C, the *sine-sine* type has much larger $\bar{C_P}$ than any other types all through the advance ratio. In comparing between the rotational times, $\bar{C_P}$ decreases with the shorter rotational time all through the advance ratio; and the *trapez-trapez* type in $\tau_r = 0.2$ has the smallest $\bar{C_P}$ in all types all through the advance ratio. This tendency is the same as in hovering flight.

As shown in Fig.11D, the *sine-sine* type has

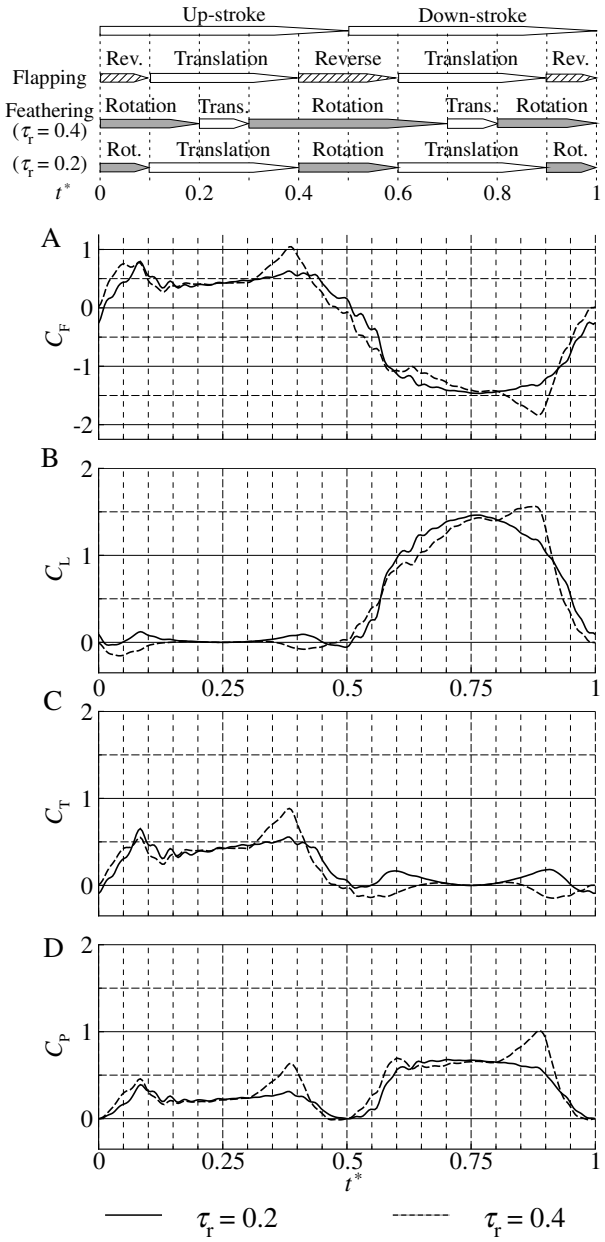

Fig. 12 Time histories of aerodynamic forces at $J = 0.20$ with the *trapez-trapez* type at $\psi = 45°$.

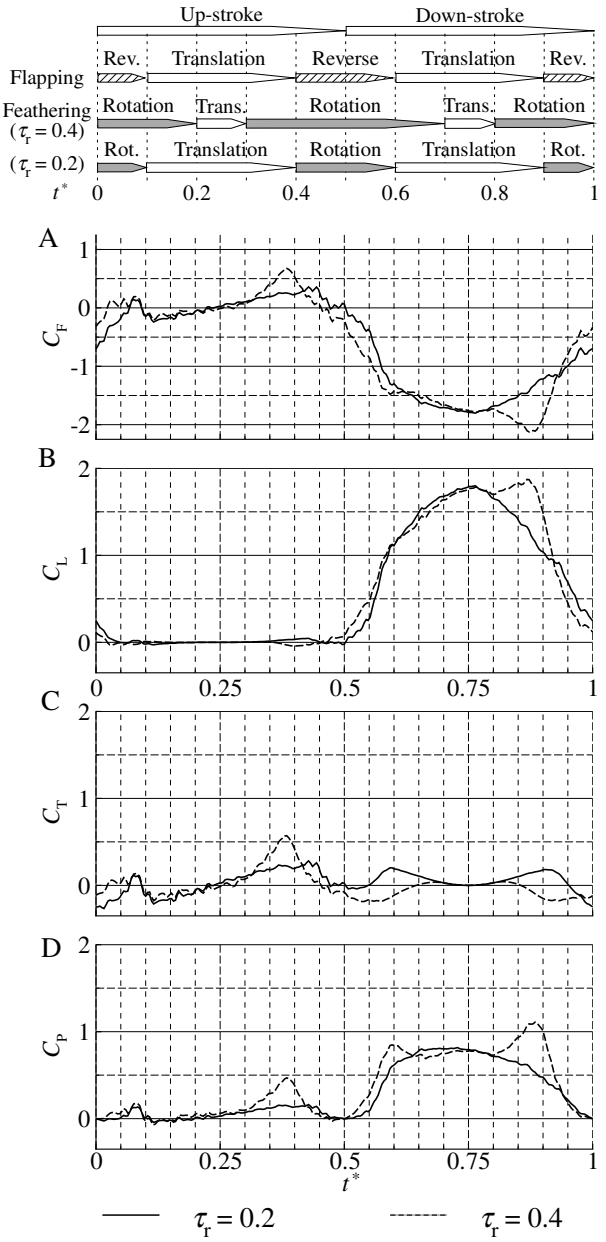

Fig. 13 Time histories of aerodynamic forces at $J = 0.47$ with the *trapez-trapez* type at $\psi = 45°$.

the smallest $\bar{C_L}/\bar{C_P}$ in all types all through the advance ratio. In comparing between the rotational times, $\bar{C_L}/\bar{C_P}$ increases with the shorter rotational time all through the advance ratio; and the *trapez-trapez* type in $\tau_r = 0.2$ has the largest $\bar{C_L}/\bar{C_P}$ all through the advance ratio. This tendency is the same as in hovering flight. In Fig. 11E, let us pay attention only to the area of $\eta > 0$. η has a maximum at an advance ratio about $J = 0.25 - 0.3$. The *sine-sine* type has the smallest η and the *trapez-trapez* type has the larger η.

4.2 Discussion of time histories of forces

Figures 12 and 13 show the time histories of aerodynamic forces at $J = 0.20$ and 0.47, respectively, at $\psi = 45°$ with the *trapez-trapez* type in $\tau_r = 0.2$ and 0.4. In forward flight, a flapping wing experiences the different relative flow velocity and ef-

fective angle of attack between the up- and down-stroke unlike in hovering flight, because of the forward velocity and the inclined stroke plane. Thus, the fluid force is enhanced in the down-stroke and reduced in the up-stroke.

Once the rotational phase of $\tau_r = 0.4$ begins (see $0.3 < t^* < 0.4$ and $0.8 < t^* < 0.9$ in Figs.12A and 13A), C_F in $\tau_r = 0.4$ increases rapidly due to the rotational effect; at the same time, C_P also increases rapidly (see Figs.12D and 13D). The combination of the rotational phase with the flapping translational phase needs much more power though lift and thrust increase, like in hovering flight.

In the acceleration of the reversal phase in the up-stroke (see $0.0 < t^* < 0.1$ in Figs.12A and 13A), C_F has a peak because of the acceleration and the wake capture, like in hovering flight. However, in the acceleration in the down-stroke ($0.5 < t^* < 0.6$), there is no peak of C_F, unlike in hovering flight. In addition, C_F at the reversal from the up- to down-stroke ($t^* = 0.5$) is different from that at the reversal from the down- to up-stroke ($t^* = 1.0$), in particular case of $\tau_r = 0.2$, despite with exactly the same relative flow and attitude of the wing. For example, C_F is about -0.7 at $t^* = 1.0$ whereas it is about zero at $t^* = 0.5$ as shown in Fig.13A. These phenomena are quite different from that in hovering flight. These results indicate that there is a difference of wake capture effect between at the two reversals due to the forward velocity.

For obtaining larger lift and thrust in forward flight, it is important not only to enhance the normal force but also to consider the instantaneous attitude of the wing. As shown in Figs.12B and C, the enhanced normal force due to the rotational effect of $\tau_r = 0.4$ results in negative lift in the up-stroke and negative thrust in the down-stroke because of the bad attitude of the wing; on the other hand, C_L and C_T in $\tau_r = 0.2$ result in positive in both up- and down-stroke. As a result, $\bar{C_L}$ and $\bar{C_T}$ in $\tau_r = 0.2$ are larger than those in $\tau_r = 0.4$ at $J = 0.20$, as shown in Figs.11A and B. The discrepancy of the waveforms of C_L between $\tau_r = 0.2$ and 0.4 is smaller at $J = 0.47$ than that at $J = 0.20$, except for the range of $0.8 < t^* < 1.0$. As a result, $\bar{C_L}$ in $\tau_r = 0.4$ is larger than that in $\tau_r = 0.2$ at $J = 0.47$ unlike the result at $J = 0.20$, as shown in Fig.11A. With increasing the advance ratio, the up-stroke is little effective on lift because the relative flow and the effective angle of attack decrease. On the contrary, the relative flow velocity in the down-stroke is enhanced with increasing the advance ratio, in particular, in the middle of the stroke. This fact indicates that the contribution of the reversal phase to lift is relatively reduced. Thus, the combination of the rotational phase with the reversal phase is little effective on the increase of lift, although it is still effective on the increase of efficiency. Thrust varies from negative to positive in the up-stroke at $J = 0.47$ as shown in Fig.13C. In this case, some section of the wing experience back-flow condition due to the faster forward velocity.

5 Conclusions

We measured the aerodynamic characteristics of the flapping wing in hovering and forward flights using the dynamically scaled mechanical model in the water tunnel, and investigated the effects of motion types of flapping kinematics. In order to obtain higher efficiency in hovering and forward flights, the trapezoidal type of flapping motion and the trapezoidal type of feathering motion with the shorter rotational time should be selected. In order to obtain larger lift in hovering and forward flights at lower advance ratios, the sinusoidal type of flapping motion and the trapezoidal type of feathering motion with the shorter rotational time should be selected; in forward flight at higher advance ratios, the sinusoidal type of flapping motion and the sinusoidal type of feathering motion should be selected.

Acknowledgements

Authors acknowledge the support of Ministry of Education, Culture, Sports, Science and Technology of Japan under the High-Tech Research Center Promotion Program. And authors acknowledge the support of Professor Hiroyasu Akahoshi of Kyushu Institute of Technology.

References

[1] Dickinson, M. H., Lehmann, F. -O. and Sane, S. P. Wing rotation and the aerodynamic basis of insect flight. *Science*, 284, pp 1954-1960, 1999.

[2] Dickson, W. B. and Dickinson, M. H. The effect of advance ratio on the aerodynamics of revolving wing. *J. Exp. Biol.*, 207, pp 4269-4281, 2004.

[3] Sun, M. and Tang, J. Lift and power requirements of hovering flight in Drosophila virilis. *J. Exp. Biol.*, 205, pp 2413-2427, 2002.

[4] Yamamoto, M. and Isogai, K. Measurement of unsteady fluid dynamic forces for a mechanical dragonfly model. *J. AIAA*, Vol. 43, No. 12, pp 2475-2480, 2005.

[5] Wu, J. and Sun, M. Unsteady aerodynamic forces and power requirements of a bumblebee in forward flight. *Acta Mech Sinica*, Vol. 21, pp 207-217, 2005.

[6] Dudley, R., and Ellington, C. P. Mechanics of Forward Flight in Bumblebees I. Kinematics and Morphology. *J. Exp. Biol.*, 148, pp 19-52, 1990.

Copyright Statement